arXiv:cond-mat/0010275v1 [cond-mat.str-el] 19 Oct 2000

One-loop approximation for the Heisenberg antiferromagnet

A. Sherman
Institute of Physics, University of Tartu, Riia 142, 51014 Tartu, Estonia

M. Schreiber
Institut für Physik, Technische Universität, D-09107 Chemnitz, Federal Republic of Germany

(February 1, 2008)

We use the diagram technique for spin operators to calculate Green's functions and observables of the spin-$\frac{1}{2}$ quantum Heisenberg antiferromagnet on a square lattice. The first corrections to the self-energy and interaction are taken into account in the chain diagrams. The approximation reproduces main results of Takahashi's modified spin-wave theory [Phys. Rev. B **40**, 2494 (1989)] and is applicable in a wider temperature range. The energy per spin calculated in this approximation is in good agreement with the Monte Carlo and small-cluster exact-diagonalization calculations in the range $0 \leq T \lesssim 1.2J$ where J is the exchange constant. For the static uniform susceptibility the agreement is good for $T \lesssim 0.6J$ and becomes somewhat worse for higher temperatures. Nevertheless the approximation is able to reproduce the maximum in the temperature dependence of the susceptibility near $T = 0.9J$.

PACS numbers: 75.30.Ds, 75.50.Ee

I. INTRODUCTION

Properties of the spin-$\frac{1}{2}$ quantum Heisenberg antiferromagnet on a square lattice have attracted much attention in connection with the investigation of cuprate-perovskite high-temperature superconductors. Much of this interest stems from Anderson's original suggestion[1] that quantum spin fluctuation in CuO_2 planes of these compounds may be responsible for superconductivity. At present it is generally accepted that the undoped CuO_2 planes are well described by the Heisenberg model with nearest-neighbor interaction (see Ref. 2 and references therein).

Numerical calculations[3,4] and the analysis of experimental data[5] presented strong evidence that the two-dimensional nearest-neighbor $s = \frac{1}{2}$ Heisenberg antiferromagnet has long-range order at zero temperature. For $T \neq 0$ the Hohenberg-Mermin-Wagner theorem[6] shows rigorously that long-range order is destroyed. In real quasi-two-dimensional cuprate perovskites long-range order persists for temperatures lower than the Néel temperature. In this case the ordering is destroyed by small concentrations of carriers $x \lesssim 0.01$.[2] In both cases there is a range of parameters where the arising short-range order is characterized by the magnetic correlation length ξ which is much larger than the in-plane intersite distance a. In this situation, the spin-wave theories[7–9] modified for short-range order may be a good starting point for the investigation of antiferromagnets.[10] For undoped crystals observables calculated in these theories agree nicely (cp. Refs. 7–9) with the small-cluster exact-diagonalization and Monte Carlo data up to temperature $T \approx 0.6J$ where J is the exchange constant. This corresponds to the correlation length $\xi \approx 10a$.[7,8] However, in cuprates for the region of carrier concentrations $x \gtrsim 0.1$, which is of prime

interest, ξ is of the order of few lattice spacings.[11] In this case the application of the modified spin-wave theories (MSWT) becomes doubtful.

In this paper we extend the analytic description of elementary excitations of the undoped antiferromagnet to the region of higher temperatures and shorter correlation lengths. For this purpose we use the diagram technique for spin operators, developed in Ref. 12 (see also Ref. 13). We consider the first corrections to the simplest chain diagrams. Due to peculiar shapes of the main correction diagrams this approximation will be referred to as the one-loop approximation (OLA). We note that the OLA is not rotationally invariant (neither is the MSWT).

As will be seen below, the obtained formulas are in many respects similar to the formulas of the MSWT developed in Refs. 7,8. The major difference between these two approximations is in the evaluation of the excitation frequency. In the MSWT two parameters defining the frequency are deduced from the constraint of zero site magnetization and a self-consistency condition, while in the OLA these parameters are determined from the values of diagrams. The OLA reproduces the main results of the MSWT and is applicable in a wider temperature range. The energy per spin calculated in the OLA agrees nicely with the Monte Carlo and small-cluster exact-diagonalization calculations up to $T \approx 1.2J$. In the temperature range $T \lesssim 0.6J$ both approximations give values of the static uniform susceptibility in good agreement with numerical calculations. In the OLA, the agreement becomes somewhat worse for larger temperatures. Nevertheless this approximation is able to reproduce the maximum in the temperature dependence of the susceptibility near $T = 0.9J$ in close correspondence with experiment and numerical calculations, while in the MSWT the susceptibility grows monotonously with temperature.

It is worth noting also that the OLA reproduces results of the traditional spin-wave approximation on the zero-temperature renormalization of the excitation frequency and of the renormalization group theory[5] on the temperature variation of the correlation length. We have found also good agreement between data on zero-temperature spin correlations obtained with the projected Monte Carlo simulations, the MSWT of Ref. 9, and the present OLA.

The outline of the paper is as follows. In Sec. II the diagram technique for spin operators is discussed. The series of the simplest chain diagrams is summed in Sec. III. At $T = 0$ this approximation is similar to the spin-wave approximation suggested by Anderson.[14] The one-loop corrections to the chain diagrams are considered in Sec. IV. The obtained excitation spectrum is compared here and in Sec. V with the spectra of the traditional spin-wave theory and the MSWT. The spin-wave approximation based on the obtained formulas is discussed in Sec. V. Here results of the OLA for the energy, susceptibility and spin correlations are compared with exact-diagonalization, Monte Carlo, and MSWT data. Our summary is given in Sec. VI.

II. DIAGRAM TECHNIQUE

The Hamiltonian of the Heisenberg antiferromagnet can be written in the form

$$H = \sum_{\mathbf{lm}} J_{\mathbf{lm}} \mathbf{s_l} \mathbf{s_m} = \sum_{\mathbf{lm}} J_{\mathbf{lm}} \left[s^z_{\mathbf{l}} s^z_{\mathbf{m}} + \frac{1}{2} \left(s^+_{\mathbf{l}} s^-_{\mathbf{m}} + s^-_{\mathbf{l}} s^+_{\mathbf{m}} \right) \right], \quad (1)$$

where $\mathbf{l}$ and $\mathbf{m}$ label the sites of the two sublattices of the square lattice, the exchange constants $J_{\mathbf{lm}}$ are expected to be nonzero for nearest neighbor sites only, $J_{\mathbf{lm}} = J \sum_{\mathbf{a}} \delta_{\mathbf{l},\mathbf{m}+\mathbf{a}}$ with $\mathbf{a} = (0, \pm a), (\pm a, 0)$, $\mathbf{s_l}$ is the spin-$\frac{1}{2}$ operator the components of which satisfy the commutation relations

$$[s^x_{\mathbf{n}}, s^y_{\mathbf{n}'}] = i s^z_{\mathbf{n}} \delta_{\mathbf{nn}'}, \quad (2)$$

and analogously for cyclic permutations of indices x, y and z. Here $\mathbf{n} = \mathbf{l}$ or $\mathbf{m}$ and $s^{\pm}_{\mathbf{n}} = s^x_{\mathbf{n}} \pm i s^y_{\mathbf{n}}$. For $s = \frac{1}{2}$ we have $s^z_{\mathbf{n}} = -\frac{1}{2} + s^+_{\mathbf{n}} s^-_{\mathbf{n}}$ and $s^+_{\mathbf{n}} s^-_{\mathbf{n}} + s^-_{\mathbf{n}} s^+_{\mathbf{n}} = 1$.

On one sublattice we change notations: $s^{\mp}_{\mathbf{m}} = -\tilde{s}^{\pm}_{\mathbf{m}}$ and $s^z_{\mathbf{m}} = -\tilde{s}^z_{\mathbf{m}} = \frac{1}{2} - \tilde{s}^+_{\mathbf{m}} \tilde{s}^-_{\mathbf{m}}$. The new operators $\tilde{s}^{\alpha}_{\mathbf{m}}$ satisfy commutation relations (2). Substituting the new notations in Hamiltonian (1) and omitting the tildes we find

$$H = -\frac{JN}{2} + H_0 + H_1,$$
$$H_0 = 2J \left(\sum_{\mathbf{l}} s^+_{\mathbf{l}} s^-_{\mathbf{l}} + \sum_{\mathbf{m}} s^+_{\mathbf{m}} s^-_{\mathbf{m}} \right), \quad (3)$$
$$H_1 = -\sum_{\mathbf{lm}} J_{\mathbf{lm}} \left[s^+_{\mathbf{l}} s^-_{\mathbf{l}} s^+_{\mathbf{m}} s^-_{\mathbf{m}} + \frac{1}{2} \left(s^+_{\mathbf{l}} s^+_{\mathbf{m}} + s^-_{\mathbf{l}} s^-_{\mathbf{m}} \right) \right],$$

where N is the number of lattice sites.

Our aim is the calculation of Green's functions

$$D_{\mathbf{ll}'}(\tau) = -\langle \mathcal{P} s^-_{\mathbf{l}}(\tau) s^+_{\mathbf{l}'} \rangle,$$
$$D'_{\mathbf{lm}}(\tau) = -\langle \mathcal{P} s^-_{\mathbf{l}}(\tau) s^-_{\mathbf{m}} \rangle,$$
$$D''_{\mathbf{ml}}(\tau) = -\langle \mathcal{P} s^+_{\mathbf{m}}(\tau) s^+_{\mathbf{l}} \rangle,$$

where $s^-_{\mathbf{l}}(\tau) = \exp(H\tau) s^-_{\mathbf{l}} \exp(-H\tau)$, the time-ordering operator $\mathcal{P}$ arranges operators in order of increasing time from right to left, and angular brackets denote thermodynamic averaging with the Hamiltonian H. It follows from the above definition that $[D'_{\mathbf{lm}}(\tau)]^* = D''_{\mathbf{ml}}(\tau)$.

Using H_0 and H_1 from Eq. (3) as the unperturbed Hamiltonian and perturbation, respectively, Green's functions can be represented by an infinite series generated by the known series of the evolution operator. The terms of the former series contain Green's functions

$$\langle \mathcal{P} s^{\alpha_1}_{\mathbf{n}_1}(\tau_1) s^{\alpha_2}_{\mathbf{n}_2}(\tau_2) \dots s^{\alpha_p}_{\mathbf{n}_p}(\tau_p) \rangle_0 \quad (4)$$

where the averaging and time dependences of the operators are determined with the unperturbed Hamiltonian

H_0 as indicated by the subscript 0 of the angular brackets, so that

$$s^{\pm}_{\mathbf{n}}(\tau) = s^{\pm}_{\mathbf{n}} e^{\pm 2J\tau}.$$

As follows from Eq. (3), Green's functions (4) contain only operators s^+ and s^- (i.e. $\alpha_i = +$ or $-$) and do not contain operators s^z. These Green's functions are nonzero when the number of s^- operators is equal to the number of s^+ operators. To calculate these functions we use Wick's theorem proposed for spin operators in Ref. 12 (see also Ref. 13). The theorem can be written in the form

$$\begin{aligned}
&\langle \mathcal{P} s^{\alpha_1}_{\mathbf{n}_1}(\tau_1) \dots s^{-}_{\mathbf{n}}(\tau) \dots s^{\alpha_p}_{\mathbf{n}_p}(\tau_p)\rangle_0 \\
&\quad = K(\tau-\tau_1)\langle \mathcal{P}\left[s^{-}_{\mathbf{n}}, s^{\alpha_1}_{\mathbf{n}_1}\right]_{\tau_1} \dots s^{\alpha_p}_{\mathbf{n}_p}(\tau_p)\rangle_0 + \dots \\
&\quad + K(\tau-\tau_p)\langle \mathcal{P} s^{\alpha_1}_{\mathbf{n}_1}(\tau_1) \dots \left[s^{-}_{\mathbf{n}}, s^{\alpha_p}_{\mathbf{n}_p}\right]_{\tau_p}\rangle_0
\end{aligned} \tag{5}$$

where

$$K(\tau) = e^{-2J\tau}\left(1-e^{-2J\beta}\right)^{-1} \begin{cases} 1, & \tau > 0 \\ e^{-2J\beta}, & \tau < 0 \end{cases}$$

and $\beta^{-1} = T$ is the temperature. The subscripts τ_i of the commutators in Eq. (5) are the time arguments of the operators arising after the commutations. Equation (5) is easily verified by transferring $s^-_{\mathbf{n}}(\tau)$ to the right averaging bracket with the introduction of the commutators, using cyclic permutation in the averaging and transferring the operator from the left bracket to its initial position.

As noted above, terms (4) in the series expansion of Green's functions contain only operators s^- and s^+. However, after the application of Wick's theorem (5) operators s^z appear in the averaging. Equation (5) is also applicable, if some of the s^{α_i} are s^z operators and the couplings of s^- with s^z have to be taken into account along with the coupling of the former operators with s^+. Equation (5) is used until only operators s^z are left in the averaging brackets. Since the Hamiltonian H_0 is the sum of terms related to individual sites, these averages are split into averages related to individual sites. Such averages are easily calculated using the recurrence relation

$$\left\langle \left(s^z_{\mathbf{n}}\right)^{k+1}\right\rangle_0 = \left\langle \left(s^z_{\mathbf{n}}\right)^{k}\right\rangle_0 \langle s^z_{\mathbf{n}}\rangle_0 - \frac{1}{2\beta}\frac{\partial}{\partial J}\left\langle \left(s^z_{\mathbf{n}}\right)^{k}\right\rangle_0, \tag{6}$$

$$\langle s^z_{\mathbf{n}}\rangle_0 = -\frac{1}{2}\tanh(J\beta) \equiv -\frac{c}{2}.$$

For the following discussion we notice that

$$\langle s^z_{\mathbf{n}} s^z_{\mathbf{n}'}\rangle_0 = \langle s^z_{\mathbf{n}}\rangle_0^2 - \frac{1}{2\beta}\frac{\partial}{\partial J}\langle s^z_{\mathbf{n}}\rangle_0 \delta_{\mathbf{n}\mathbf{n}'}, \tag{7a}$$

$$\begin{aligned}
\langle s^z_{\mathbf{n}} s^z_{\mathbf{n}'} s^z_{\mathbf{n}''}\rangle_0 &= \langle s^z_{\mathbf{n}}\rangle_0^3 \\
&- \langle s^z_{\mathbf{n}}\rangle_0 \frac{1}{2\beta}\frac{\partial}{\partial J}\langle s^z_{\mathbf{n}}\rangle_0 \left(\delta_{\mathbf{n}\mathbf{n}'} + \delta_{\mathbf{n}\mathbf{n}''} + \delta_{\mathbf{n}'\mathbf{n}''}\right) \\
&+ \frac{1}{4\beta^2}\frac{\partial^2}{\partial J^2}\langle s^z_{\mathbf{n}}\rangle_0 \delta_{\mathbf{n}\mathbf{n}'}\delta_{\mathbf{n}\mathbf{n}''},
\end{aligned} \tag{7b}$$

where we took into account that $\langle s^z_{\mathbf{n}}\rangle_0$ and its derivatives do not depend on $\mathbf{n}$. Analogous formulas can be written for an average of a larger number of s^z operators.

The diagram technique can be used to visualize the terms of the perturbation theory.[12,13] $K(\tau-\tau')$ will be displayed graphically by a solid line with an arrow directed from τ to τ' [from the respective s^- to s^+ or s^z operators, see Eq. (5)]. An s^z operator is connected with the terminal point of this line unless a second line with an arrow enters into this point. This latter case corresponds to the situation when an s^z operator which appears after the commutation of s^- and s^+ operators participates in another coupling. The s^- operator produced in this way participates in further couplings and therefore a third line has to issue from the terminal point of the former two lines (see Fig. 1a).

Excluding two free points labelled by the time arguments τ and 0 all other initial and terminal points of the directed lines are connected by wavy lines corresponding to the exchange integrals $J_{\mathbf{lm}}$ in the longitudinal [the first term in H_1, Eq. (3)] and transverse interactions (the second and third terms in H_1). The transverse interaction line connects two directed lines, either terminating or initiating (Fig. 1b and c). The longitudinal interaction line connects four directed lines, one terminating and one initiating at each end of the interaction line (Fig. 1d).

The delta functions in the last terms of Eqs. (7a) and (7b) introduce limitations on the site indices of the s^z operators. In the diagrams we shall denote these limitations by dashed lines connecting ends of directed lines (points corresponding to s^z operators). A second-order diagram with such a dashed line arising due to the second term on the right-hand side of Eq. (7a) is shown in Fig. 1e. As usual the partition function in the denominators of Green's functions cancels all unlinked diagrams. It must be noted that a dashed line can connect an otherwise unlinked diagram, as shown in Fig. 1e.

III. CHAIN DIAGRAMS

A satisfactory description of low-temperature excitations of the Heisenberg antiferromagnet is achieved in the Anderson approximation[14] which neglects the longitudinal interaction and substitutes the spin operators s^+ and s^- by Boson annihilation and creation operators. In the diagram representation this approximation is reduced to neglecting diagrams with longitudinal interaction lines and with dashed lines or loops formed by directed and transversal wavy lines (these two latter elements arise due to the non-Boson statistics of spin operators; it has to be noted that the loops contain the "triple points" similar to that shown in Fig. 1a). The remaining chain diagrams for $D_{\mathbf{ll}'}(\tau)$ are shown in Fig. 2.

After the Fourier transformation

$$D(\mathbf{k},i\omega_n)=\int_0^\beta d\tau\sum_{\mathbf{l}}e^{i\omega_n\tau}e^{i\mathbf{k}(\mathbf{l}-\mathbf{l}')}D_{\mathbf{ll}'}(\tau),$$

where $\omega_n = \pi T n$ is Matsubara's frequency with an even integer n, the series of chain diagrams can be written as

$$\begin{aligned} D^c(\mathbf{k}, i\omega_n) &= -cK(i\omega_n)\Bigg\{1 + \left(\frac{cJ_\mathbf{k}}{2}\right)^2 K(-i\omega_n)K(i\omega_n) \\ &\quad + \left[\left(\frac{cJ_\mathbf{k}}{2}\right)^2 K(-i\omega_n)K(i\omega_n)\right]^2 + \ldots\Bigg\} \\ &= \frac{c\,(i\omega_n + 2J)}{(i\omega_n)^2 - \omega_\mathbf{k}^2}, \\ D'^c(\mathbf{k}, i\omega_n) &= -\frac{J_\mathbf{k}}{2}c^2 K(i\omega_n)K(-i\omega_n) \\ &\quad \times\Bigg\{1 + \left(\frac{cJ_\mathbf{k}}{2}\right)^2 K(-i\omega_n)K(i\omega_n) \\ &\quad + \left[\left(\frac{cJ_\mathbf{k}}{2}\right)^2 K(-i\omega_n)K(i\omega_n)\right]^2 + \ldots\Bigg\} \\ &= \frac{1}{2}\frac{c^2 J_\mathbf{k}}{(i\omega_n)^2 - \omega_\mathbf{k}^2}, \end{aligned} \tag{8}$$

where

$$K(i\omega_n) = -\left(i\omega_n - 2J\right)^{-1}, \quad J_\mathbf{k} = 4J\gamma_\mathbf{k}$$

are the Fourier transforms of $K(\tau)$ and $J_{\mathbf{lm}}$, respectively, $\gamma_\mathbf{k} = \sum_\mathbf{a} \exp(i\mathbf{ka})/4$ and the excitation frequency

$$\omega_\mathbf{k} = 2J\sqrt{1 - c^2\gamma_\mathbf{k}^2}. \tag{9}$$

At $T = 0$ when $c = 1$ [see Eq. (6)] Eq. (9) reproduces the spin-wave spectrum of Ref. 14. For nonzero temperature $c < 1$ and a gap opens near $\mathbf{k} = 0$. This gap is exponentially small for low temperatures $J\beta \gg 1$.

IV. FIRST CORRECTIONS

The first corrections to the chain diagrams contain one longitudinal interaction line, a loop with the "triple point" or a dashed line in the self-energy or in the renormalized interaction. Similar corrections were considered for the case of a three-dimensional antiferromagnet and zero temperature in Ref. 15 with the use of another diagram technique and for a ferromagnet in Refs. 12,13,16. The respective diagrams are shown in Fig. 3. Diagrams (a) and (b) are self-energy corrections which are inserted in directed lines of the chain diagrams. Following Ref. 15 we carried out partial summations in these diagrams: the line with two arrows indicates the series of chain diagrams (8). Diagrams (d) to (f) are related to terminal points of directed lines and we include them together with diagram (c) to the renormalization of the interaction lines in the chain diagrams. However, in the chain diagrams the number of directed lines exceeds by one the number of wavy lines. Therefore the renormalized Green's functions

have the additional multiplier $\alpha = 1+\sigma_d+\sigma_e+\sigma_f$ where σ_i is the contribution of the ith diagram in Fig. 3. Notice that the multiplier α was not included in Refs. 15,16.

With these corrections Green's functions read

$$D(\mathbf{k}, i\omega_n) = \frac{\alpha c\,(i\omega_n + 2J\varepsilon)}{(i\omega_n)^2 - \Omega_{\mathbf{k}}^2},$$
$$D'(\mathbf{k}, i\omega_n) = \frac{2J\alpha c^2 \phi\gamma_{\mathbf{k}}}{(i\omega_n)^2 - \Omega_{\mathbf{k}}^2}, \tag{10}$$

where

$$\Omega_{\mathbf{k}} = 2J\sqrt{\varepsilon^2 - (c\phi\gamma_{\mathbf{k}})^2}, \tag{11}$$
$$\varepsilon = 1 + c^2(1 - I_1) + cI, \tag{12}$$
$$\phi = 1 + c^2 I + \frac{1}{c^2}(1 - cI_1) - \cosh^{-2}(J\beta)I' + J\beta\cosh^{-2}(J\beta)I, \tag{13}$$
$$\alpha = 1 + \frac{1}{c^2}(1 - cI_1) - \cosh^{-2}(J\beta)I' + J\beta\cosh^{-2}(J\beta)I, \tag{14}$$

$$I = \frac{1}{2J}\frac{2}{N}\sum_{\mathbf{k}}\left(\frac{J_{\mathbf{k}}}{2}\right)^2 \frac{1}{\omega_{\mathbf{k}}}\coth\left(\frac{\beta\omega_{\mathbf{k}}}{2}\right), \tag{15a}$$
$$I_1 = 2J\frac{2}{N}\sum_{\mathbf{k}}\frac{1}{\omega_{\mathbf{k}}}\coth\left(\frac{\beta\omega_{\mathbf{k}}}{2}\right), \tag{15b}$$
$$I' = \frac{2}{N}\sum_{\mathbf{k}}\left(\frac{J_{\mathbf{k}}}{2}\right)^2 \frac{1}{(i\omega_n)^2 - \omega_{\mathbf{k}}^2}. \tag{15c}$$

Here and below summations over wave vectors are carried over the magnetic Brillouin zone. The second and third terms on the right-hand side of Eq. (12) are contributions of diagrams (a) and (b) in Fig. 3, respectively. The second to fifth terms on the right-hand side of Eq. (13) are contributions of diagrams (c) to (f), respectively. As mentioned, diagrams (d), (e), and (f) give the last three terms in α, Eq. (14). In the calculation of the correction introduced by diagram (c) we took into account that for any $f(\mathbf{k})$ invariant with respect to operations of the crystal point group

$$\sum_{\mathbf{k}'} J_{\mathbf{k}-\mathbf{k}'} f(\mathbf{k}') = J_{\mathbf{k}} J_{\mathbf{0}}^{-1} \sum_{\mathbf{k}'} J_{\mathbf{k}'} f(\mathbf{k}').$$

To estimate the contributions of the diagrams in Fig. 3 we introduce the function[7]

$$w(x) = \frac{2}{N}\sum_{\mathbf{k}}\delta\left(x - \gamma_{\mathbf{k}}\right),\ 0 \le x \le 1, \tag{16a}$$

and consider an infinite square lattice. In this case

$$w(x) = \left(\frac{2}{\pi}\right)^2 \mathcal{K}\left(\sqrt{1-x^2}\right) = \frac{2}{\pi} + \mathcal{O}(1-x), \tag{16b}$$

where $\mathcal{K}(k)$ is a complete elliptic integral of the first kind with modulus k. For low temperatures $T \ll J$ we find

$$
\begin{aligned}
I &= c^{-2}(I_1 - I_2), \\
I_1 &= \int_0^1 \frac{w(x)}{\sqrt{1-c^2x^2}} \coth\left(\beta J\sqrt{1-c^2x^2}\right) dx \\
&= w(1) + 2(1-m_0) - \frac{w(1)}{\beta J}\ln(4\beta J) + \mathcal{O}\left[(\beta J)^{-3}\right], \\
I_2 &= \int_0^1 w(x)\sqrt{1-c^2x^2}\coth\left(\beta J\sqrt{1-c^2x^2}\right) dx \qquad (17) \\
&= 2(1-m_1) + \frac{w(1)\zeta(3)}{2(\beta J)^3} + \mathcal{O}\left[(\beta J)^{-5}\right], \\
I' &= c^{-2}\int_0^1 \frac{w(x)x^2}{x^2 - x_0^2} dx \\
&= \frac{w(1)x_0}{2}\ln\left|\frac{1-x_0}{1+x_0}\right| + \mathcal{O}\left[(\beta J)^0\right],
\end{aligned}
$$

where

$$
\begin{aligned}
m_0 &= 1 - \frac{1}{2}\int_0^1 \frac{w(x)}{\sqrt{1-x^2}} dx \approx 0.303398, \\
m_1 &= 1 - \frac{1}{2}\int_0^1 w(x)\sqrt{1-x^2} dx \approx 0.578974, \qquad (18) \\
x_0 &= \frac{\sqrt{\omega_n^2 + 4J^2}}{2Jc},
\end{aligned}
$$

$\zeta(x)$ is the Riemann zeta function, and $\mathcal{O}\left[(\beta J)^0\right]$ in I' comprises terms slowly varying with ω_n.

From Eqs. (13), (14), (17), and (18) one can see that due to the multipliers $\cosh^{-2}(J\beta)$ for low temperatures, where the obtained formulas are expected to be valid, σ_e and σ_f are much smaller than σ_c and σ_d and therefore the two former contributions can be omitted. The retained diagrams contain a closed loop formed by directed and wavy lines [diagrams (b), (c), and (d)] or a bubble [diagram (a)]. Due to these shapes of the main diagrams we use the term "one-loop approximation". From the above equations we find that in two dimensions contributions of these separate diagrams are not small in comparison with the unperturbed self-energy and interaction. For example, the zero-temperature value of diagram (b) is $2.38J$ to be compared with the unperturbed self-energy $2J$. However, the sums of the values of the diagrams (a) and (b), as well as (c) and (d) are small in comparison with the respective unperturbed values. Substituting (17) in Eqs. (11)–(14) we find for an infinite lattice

$$
\begin{aligned}
\Omega_{\mathbf{k}} &= 2J\varepsilon\sqrt{1 - r^2\gamma_{\mathbf{k}}^2}, \\
\varepsilon &= 2m_1 - \frac{w(1)\zeta(3)}{2(\beta J)^3} + \mathcal{O}\left[(\beta J)^{-5}\right], \\
r &= c\phi\varepsilon^{-1} = 1 - 2m_1^{-1}\big\{1 + 2w(1) \qquad (19) \\
&\quad -4m_0 + 2m_1 + \mathcal{O}\left[(\beta J)^{-1}\right]\big\}\exp(-2J\beta), \\
\alpha &= 2m_0 - w(1) + \mathcal{O}\left[(\beta J)^{-1}\right].
\end{aligned}
$$

The zero-temperature renormalization of the frequencies of elementary excitations, given by Eq. (19), coincides with the result obtained previously in the traditional spin-wave approximation[17,18] and by other methods.[7–9] The temperature variation of the frequency described by the term $-0.5w(1)\zeta(3)(\beta J)^{-3}$ in Eq. (19) is close to the MSWT result[7] $-0.322w(1)\zeta(3)(\beta J)^{-3}$. For nonzero temperature $r < 1$ which produces a gap near $\mathbf{k} = 0$ in the spectrum of elementary excitations. For low temperatures the size of the gap is exponentially small and the obtained exponent $-J\beta$ is close to the MSWT value[7] $-4m_0m_1w^{-1}(1)J\beta \approx -1.1037J\beta$. However, the preexponential factors are different in these two approaches.

V. THE SPIN-WAVE APPROXIMATION

In contrast to the small correction to the excitation frequency, the numerators of Green's functions (10) are essentially renormalized in comparison with the chain approximation (8). In Eq. (19) $\alpha \approx -0.03$ and with this small multiplier Green's functions (10) nearly vanish. It is worth noting the direct analogy of this result with the MSWT[7,8] where the correlations $\left\langle s_{\mathbf{l}}^- s_{\mathbf{l}'}^+ \right\rangle$, $\left\langle s_{\mathbf{l}}^- s_{\mathbf{m}}^- \right\rangle$ and the related Green's functions are exactly zero. Thus, like this theory, the OLA is not rotationally invariant and the z components of the spin correlations are much larger than the other components. In the following discussion these latter components will be neglected.

The analogy with the MSWT may be continued, if attention is drawn to the fact that the quantities

$$d(\mathbf{k}, i\omega_n) = D(\mathbf{k}, i\omega_n)/\alpha, \quad d'(\mathbf{k}, i\omega_n) = D'(\mathbf{k}, i\omega_n)/\alpha$$

are Green's functions of spin waves. Indeed, the factor α in Green's functions (10) differs from 1 due to the terminal-point diagrams (d), (e), and (f) which account for the non-Boson statistics of spin operators corresponding to the terminal points. Thus, dropping α in Green's functions (10) corresponds to the replacement of the spin operators by the respective Boson operators of spin waves. We introduce these latter operators with the Dyson-Maleev transformation

$$s_{\mathbf{l}}^- = b_{\mathbf{l}}^\dagger,\ s_{\mathbf{l}}^+ = \left(1 - b_{\mathbf{l}}^\dagger b_{\mathbf{l}}\right) b_{\mathbf{l}},\ s_{\mathbf{l}}^z = \frac{1}{2} - b_{\mathbf{l}}^\dagger b_{\mathbf{l}},$$

$$s_{\mathbf{m}}^- = -b_{\mathbf{m}},\ s_{\mathbf{m}}^+ = -b_{\mathbf{m}}^\dagger \left(1 - b_{\mathbf{m}}^\dagger b_{\mathbf{m}}\right),\ s_{\mathbf{m}}^z = -\frac{1}{2} + b_{\mathbf{m}}^\dagger b_{\mathbf{m}}$$

(here and below we return to the initial coordinate system on the sublattice labelled by the index $\mathbf{m}$). In these notations d and d' acquire the familiar form of the magnon Green's functions

$$d_{\mathbf{l}\mathbf{l}'}(\tau) = -\left\langle \mathcal{P} b_{\mathbf{l}}^\dagger(\tau) b_{\mathbf{l}'} \right\rangle, \quad d'_{\mathbf{l}\mathbf{m}}(\tau) = -\left\langle \mathcal{P} b_{\mathbf{l}}^\dagger(\tau) b_{\mathbf{m}}^\dagger \right\rangle.$$

It is essential to note that the self-energy and interaction-line corrections, which are also connected with the non-Boson statistics of spin operators and renormalize the

excitation frequency, are taken into account in d and d'. Analogous corrections are allowed for in the MSWT and, as a consequence, d and d' derived from Eq. (10) up to the factor c coincide in their form with the magnon Green's functions obtained[9] in that theory. However, in the discussed spin-wave approximation the excitation frequency is determined by Eqs. (11)–(13), and (15). They differ from the equations[7,8] defining the frequency in the MSWT.

Taking into account that

$$\left\langle b_{\mathbf{l}}^{\dagger} b_{\mathbf{l}'} \right\rangle = -d_{\mathbf{l}\mathbf{l}'}(\tau = +0) = -\int_{\mathcal{C}} \frac{e^{-z\tau}}{1 - e^{-z\beta}} d_{\mathbf{l}\mathbf{l}'}(z) \frac{dz}{2\pi i},$$
$$\left\langle b_{\mathbf{l}'} b_{\mathbf{l}}^{\dagger} \right\rangle = -d_{\mathbf{l}\mathbf{l}'}(\tau = -0) = -\int_{\mathcal{C}} \frac{e^{-z\tau}}{e^{z\beta} - 1} d_{\mathbf{l}\mathbf{l}'}(z) \frac{dz}{2\pi i},$$

where $\mathcal{C}$ is a closed contour embracing the complex plane, we find

$$\langle \mathbf{s_l s_{l'}} \rangle = \langle s_{\mathbf{l}}^z s_{\mathbf{l}'}^z \rangle \approx \left\langle b_{\mathbf{l}}^{\dagger} b_{\mathbf{l}'} \right\rangle \left\langle b_{\mathbf{l}} b_{\mathbf{l}'}^{\dagger} \right\rangle = \left[\frac{c}{2} \frac{2}{N} \sum_{\mathbf{k}} e^{i\mathbf{k}(\mathbf{l}'-\mathbf{l})} \frac{1}{\sqrt{1 - r_{\mathbf{k}}^2 \gamma_{\mathbf{k}}^2}} \coth\left(J\beta\varepsilon \sqrt{1 - r_{\mathbf{k}}^2 \gamma_{\mathbf{k}}^2} \right) \right]^2 - \frac{c^2}{4} \delta_{\mathbf{l}\mathbf{l}'},$$
$$\langle \mathbf{s_l s_m} \rangle = \langle s_{\mathbf{l}}^z s_{\mathbf{m}}^z \rangle \approx -\langle b_{\mathbf{l}} b_{\mathbf{m}} \rangle \left\langle b_{\mathbf{l}}^{\dagger} b_{\mathbf{m}}^{\dagger} \right\rangle = -\left[\frac{c}{2} \frac{2}{N} \sum_{\mathbf{k}} e^{i\mathbf{k}(\mathbf{m}-\mathbf{l})} \frac{r_{\mathbf{k}} \gamma_{\mathbf{k}}}{\sqrt{1 - r_{\mathbf{k}}^2 \gamma_{\mathbf{k}}^2}} \coth\left(J\beta\varepsilon \sqrt{1 - r_{\mathbf{k}}^2 \gamma_{\mathbf{k}}^2} \right) \right]^2. \tag{20}$$

In the derivation of Eq. (20) we have taken into account the constraint of zero site magnetization in the paramagnetic state

$$\langle s_{\mathbf{l}}^z \rangle = \left\langle b_{\mathbf{l}}^{\dagger} b_{\mathbf{l}} \right\rangle - \frac{1}{2} = 0, \tag{21}$$

and in calculating $\left\langle b_{\mathbf{n}}^{\dagger} b_{\mathbf{n}} b_{\mathbf{n}'}^{\dagger} b_{\mathbf{n}'} \right\rangle$ we have considered only diagrams corresponding to two independent magnon Green's functions, neglecting diagrams with interaction wavy and dashed lines between these two functions.

The index $\mathbf{k}$ added to the parameter r in Eq. (20) is noteworthy. To fulfil constraint (21) we separate out the terms with $\mathbf{k} = 0$, the so-called condensation parts, in the sums in spin correlations (20) and suppose that r in the separated terms differs from the analogous parameter in terms with $\mathbf{k} \neq 0$. This latter parameter is calculated from Eqs. (12), (13), (15), and (19), whereas $r_{\mathbf{k}=0} = r'$ in the condensation parts is determined from constraint (21) which can be written in the form

$$\frac{2}{N} \frac{1}{\sqrt{1 - r'^2}} \coth\left(J\beta\varepsilon \sqrt{1 - r'^2} \right) = \frac{1 + c}{c}$$
$$- \frac{2}{N} \sum_{\mathbf{k} \neq \mathbf{0}} \frac{1}{\sqrt{1 - r^2 \gamma_{\mathbf{k}}^2}} \coth\left(J\beta\varepsilon \sqrt{1 - r^2 \gamma_{\mathbf{k}}^2} \right). \tag{22}$$

In a large lattice and at $T = 0$ the condensation parts are equal to $2m_0$, Eq. (18), and the sums in Eqs. (20) for large $L = |\mathbf{L}|$ are equal to $2m_0 + 2^{1/2} (\pi L)^{-1}$. Thus, under these conditions

$$\langle \mathbf{s_0 s_L} \rangle \approx (-1)^L \left[m_0 + \left(\sqrt{2}\pi L \right)^{-1} \right]^2, \qquad (23)$$

where $(-1)^L = +1$ or -1 depending on whether the sites $\mathbf{0}$ and $\mathbf{L}$ belong to the same or different sublattices. The value of the sublattice magnetization $m_0 \approx 0.3034$ is in good agreement with the Monte Carlo calculations.[3,4] The $1/L$ decay of the spin correlations to the square of the order parameter at zero temperature was expected in Ref. 19. For small L the zero-temperature spin correlations $\langle \mathbf{s_0 s_L} \rangle$ calculated from Eqs. (12), (13), (15), (20), and (22), are compared with the results of the projected Monte Carlo method[4] in Table I. The values agree nicely. We notice also that our spin correlations calculated to the fourth decimal place coincide with data of the MSWT of Ref. 9.

For low temperatures the asymptotic behavior of the sums in Eqs. (20) for large distances is

$$\frac{1}{\pi^2 J\beta\varepsilon} \iint \frac{d^2k}{k^2 + (2\xi)^{-2}} e^{i\mathbf{kL}} \approx \frac{2}{J\beta\varepsilon} \sqrt{\frac{\xi}{\pi L}} \exp\left(-\frac{L}{2\xi} \right),$$

with the correlation length

$$\begin{aligned} \xi/a &= \frac{r}{\sqrt{8(1-r^2)}} \\ &\approx \frac{1}{4\sqrt{2}} \left(\frac{m_1}{1 + 2w(1) - 4m_0 + 2m_1} \right)^{1/2} e^{J\beta}. \end{aligned} \qquad (24)$$

Analogous exponential temperature dependences of the correlation length were obtained earlier in a number of works (see Refs. 5,7 and references therein). The exponent $J\beta$ in Eq. (24) is close to the values $0.94J\beta$ and $2\pi m_0 m_1 J\beta \approx 1.1037 J\beta$ obtained in Refs. 5 and 7, respectively.

In Figs. 4–6 the energy per spin

$$E = 2J \langle \mathbf{s_0 s_a} \rangle \qquad (25)$$

and the static uniform susceptibility

$$\begin{aligned} \chi &= \beta \sum_{\mathbf{n}} \langle s^z_{\mathbf{0}} s^z_{\mathbf{n}} \rangle = \frac{\beta}{3} \sum_{\mathbf{n}} \langle \mathbf{s_0 s_n} \rangle \\ &= \frac{c^2\beta}{12} \left[\frac{2}{N} \sum_{\mathbf{k}} \coth^2 \left(J\beta\varepsilon \sqrt{1 - r^2_{\mathbf{k}} \gamma^2_{\mathbf{k}}} \right) - 1 \right] \end{aligned} \qquad (26)$$

calculated with Eqs. (11)–(13), (15), (20), and (22) are compared with results of Monte Carlo simulations,[20,21] the MSWT of Refs. 7,8 and the exact diagonalization of a 4×4 lattice.[7] The parameters r, ε, and r' obtained in these calculations are given in Table II. Respective parameters η and λ which define the excitation frequency in the MSWT[7] $\omega_{\mathbf{k}} = \lambda\sqrt{1 - \eta^2\gamma^2_{\mathbf{k}}}$ [cf. Eq. (19)] are also given in this table for comparison. The size dependence of χ and E calculated with the above formulas is negligible for large enough lattices — the difference between values obtained for a 64×64 lattice and those shown in

Figs. 4 and 5 for a 20×20 lattice is less than the size of the symbols in these figures.

As seen from the figures, for temperatures $T \lesssim 0.6J$ the results obtained with OLA are close to the results of the MSWT[7,8] and are in good agreement with the Monte Carlo and exact-diagonalization data. From Figs. 4 and 6 we see also that energy (25) and the related short-range correlation are well described by the OLA even for $T \gtrsim J$ where the MSWT does not work. For the susceptibility in Fig. 5 the agreement is not so good for these temperatures, however the approximation is able to reproduce the maximum in χ near $T = 0.9J$ and the decrease of the susceptibility for higher temperatures in close correspondence with experiment and Monte Carlo simulations.

As seen from Table II, the parameters r' and ε of the OLA are close to the respective parameters η and $\lambda/(2J)$ of the MSWT of Ref. 7 for low temperatures. Essential deviations begin at $T \approx 0.5J$. We notice that the value of the parameter r is large at this temperature and grows with growing T. These values of r correspond to a large gap in the excitation spectrum near $\mathbf{k} = 0$. To understand this result we notice that in the considered magnetic Brillouin zone the vicinity of the Γ point corresponds to two regions in the usual Brillouin zone which is twice as large as the magnetic one. These regions are located near the $(0, 0)$ and $(\pi/a, \pi/a)$ points. Correspondingly, a branch of elementary excitations in the usual Brillouin zone transforms into two branches in the magnetic zone. In Ref. 9 we have considered how the magnon branch, which is twofold degenerate at $T = 0$ in the magnetic Brillouin zone, splits into two branches with growing temperature. These two branches form a unified branch in the usual Brillouin zone and are related to the central part and the periphery of this zone. In Ref. 9 we have indicated that the branch with the gap near $\mathbf{k} = 0$ in the magnetic Brillouin zone corresponds to the periphery of the usual zone and the states in this branch have larger spectral intensities in the magnon Green's function in comparison with states in the second, gapless branch. In the OLA and the MSWT of Refs. 7,8 the branch does not split and for high temperatures its behavior is expected to be determined by states with larger spectral intensities. Thus, the gap mentioned above is related to the vicinity of the $(\pi/a, \pi/a)$ point in the usual Brillouin zone.

VI. SUMMARY

In this paper we used the diagram technique for spin operators[12,13] to calculate Green's functions and observables of the undoped spin-$\frac{1}{2}$ quantum Heisenberg antiferromagnet on a square lattice. We considered the first corrections – the one-loop diagrams – to the simplest chain diagrams. The obtained equations resemble the formulas of the modified spin-wave theory of Refs. 7,8. The ma-

jor difference between these two approximations is in the calculation of the excitation frequency — in the modified spin-wave theory two parameters defining the frequency are deduced from the constraint of zero site magnetization and a self-consistency condition, while in the one-loop approximation these parameters are determined from the values of the diagrams. The one-loop approximation reproduces the results of the traditional spin-wave approximation[17,18] on the zero-temperature renormalization of the excitation frequency, of the renormalization-group theory[5] on the temperature variation of the correlation length, and of the modified spin-wave theory[7,8] on spin correlations. Due to the mentioned difference in the excitation frequency and some other differences in formulas, the one-loop approximation is applicable in a wider temperature range than the modified spin-wave theory. The energy per spin calculated in this approximation is in good agreement with the Monte Carlo and small-cluster exact-diagonalization data up to the temperatures $T \approx 1.2J$, whereas the modified spin-wave approximation gives quantitatively correct values of this energy in the range $T \lesssim 0.6J$. In this temperature range both approximations give values of the static uniform susceptibility in good agreement with numerical calculations. In the one-loop approximation, the agreement becomes somewhat worse for larger temperatures. Nevertheless this approximation is able to describe the maximum in the temperature dependence of this observable near $T = 0.9J$ in close correspondence with experiment and Monte Carlo simulations, while in the modified spin-wave theory[7,8] the susceptibility grows monotonously with temperature.

ACKNOWLEDGMENTS

This work was partially supported by the ESF grant No. 4022 and by the WTZ grant (Project EST-003-98) of the BMBF.

[1] P. W. Anderson, Science **235**, 1196 (1987).
[2] R. J. Birgeneau and G. Shirane, in: *Physical Properties of High Temperature Superconductors,* ed. D. M. Ginsberg (World Scientific, Singapore, 1989).
[3] J. D. Reger and A. P. Young, Phys. Rev. B **37**, 5978 (1988).
[4] S. Liang, Phys. Rev. B **42**, 6555 (1990).
[5] S. Chakravarty, B. I. Halperin, and D. R. Nelson, Phys. Rev. B **39**, 2344 (1989).
[6] N. D. Mermin and H. Wagner, Phys. Rev. Lett. **17**, 1133 (1966); P. C. Hohenberg, Phys. Rev. **158**, 383 (1967).
[7] M. Takahashi, Phys. Rev. B **40**, 2494 (1989).
[8] S. Tang, M. E. Lazzouni, and J. E. Hirsch, Phys. Rev. B **40**, 5000 (1989).

[9] A. Sherman and M. Schreiber, Phys. Rev. B **60**, 10180 (1999).
[10] A. Sherman and M. Schreiber, in: *Studies of High Temperature Superconductors*, vol. 27, p. 163, ed. A. V. Narlikar (Nova Science Publishers, New York, 1999); cond-mat /9808087.
[11] Y. Zha, V. Barzykin, and D. Pines, Phys. Rev. B **54**, 7561 (1996).
[12] V. G. Vaks, A. I. Larkin, and S. A. Pikin, Zh. Eksp. Teor. Fiz. **53**, 281 (1967) [Sov. Phys. JETP **26**, 188 (1968)]; **53**, 1089 (1967) [**26**, 647 (1968)].
[13] Yu. A. Izyumov and Yu. N. Skryabin, *Statistical Mechanics of Magnetically Ordered Systems* (Consultants Bureau, New York, 1988).
[14] P. W. Anderson, Phys. Rev. **86**, 694 (1952).
[15] Y. L. Wang, S. Shtrikman, and H. Callen, Phys. Rev. **148**, 419 (1966).
[16] W. W. Lewis and R. B. Stinchcombe, Proc. Phys. Soc. **92**, 1002, 1010 (1967).
[17] T. Oguchi, Phys. Rev. **117**, 117 (1960).
[18] J. Igarashi and A. Watabe, Phys. Rev. B **43**, 13456 (1991).
[19] D. A. Huse, Phys. Rev. B **37**, 2380 (1988).
[20] M. S. Makivić and H.-Q. Ding, Phys. Rev. B **43**, 3562 (1991).
[21] Y. Okabe and M. Kikuchi, J. Phys. Soc. Japan **57**, 4351 (1988).

FIG. 1. Elements of diagrams. See text for an explanation of the different lines.

FIG. 2. Chain diagrams for $D_{\mathbf{l}\mathbf{l}'}(\tau)$.

FIG. 3. The lowest-order corrections to self-energies and interaction lines.

FIG. 4. The energy per spin obtained in the Monte Carlo simulation[20] (•), in the modified spin-wave theory of Refs. 7,8 (○) and in the one-loop approximation of the present work (×). In the modified spin-wave and one-loop calculations a 20×20 lattice was used.

FIG. 5. The static uniform susceptibility obtained in the Monte Carlo simulation for a 12×12 lattice[21] (•), in the modified spin-wave theory of Refs. 7,8 (○) and in the one-loop approximation of the present work (×). In the modified spin-wave and one-loop calculations a 20×20 lattice was used.

FIG. 6. The energy per spin obtained by exact diagonalization of a 4×4 lattice[7] (•) and in the one-loop approximation (×).

TABLE I. The zero-temperature spin correlations $\langle \mathbf{s_0 s_L} \rangle$ obtained with the one-loop approximation (OLA) for a 20×20 lattice in comparison with the projected Monte Carlo data (PMC).[4]

L	PMC	OLA
$(a,0)$	-0.3348	-0.3354
(a,a)	0.2028	0.2016
$(2a,0)$	0.1772	0.1751
$(2a,a)$	-0.1671	-0.1648
$(2a,2a)$	0.1475	0.1454
$(3a,0)$	-0.1491	-0.1461
$(3a,a)$	0.1430	0.1404

TABLE II. Parameters r, ε, r' in the one-loop approximation (OLA) and the respective parameters of the modified spin-wave theory[7,8] (MSWT). In both calculations a 20×20 lattice was used.

	OLA			MSWT	
T/J	$1-r$	ε	$1-r'$	$1-\eta$	$\lambda/(2J)$
0.01	0.8634E-04	1.1582	0.4192E-04	0.4193E-04	1.1582
0.1	0.8633E-03	1.1583	0.3188E-03	0.3197E-03	1.1583
0.2	0.1860E-02	1.1561	0.6434E-03	0.6480E-03	1.1570
0.3	0.6692E-02	1.1490	0.9904E-03	0.1038E-02	1.1516
0.4	0.2528E-01	1.1385	0.1276E-02	0.1566E-02	1.1374
0.5	0.5953E-01	1.1257	0.1508E-02	0.2404E-02	1.1097
0.6	0.1033	1.1101	0.1735E-02	0.4081E-02	1.0629
0.7	0.1511	1.0928	0.1976E-02	0.8882E-02	0.98897
0.8	0.1995	1.0752	0.2230E-02	0.2930E-01	0.87371
0.9	0.2467	1.0589	0.2498E-02		
1.0	0.2918	1.0446	0.2774E-02		
1.1	0.3344	1.0327	0.3055E-02		
1.2	0.3743	1.0234	0.3336E-02		

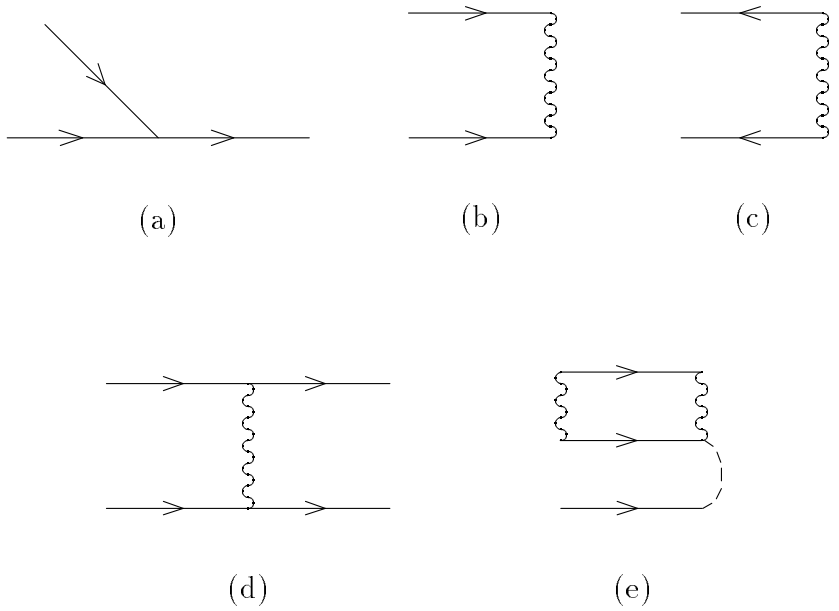

Fig. 1. A. Sherman and M.Schreiber, One-loop approximation ...

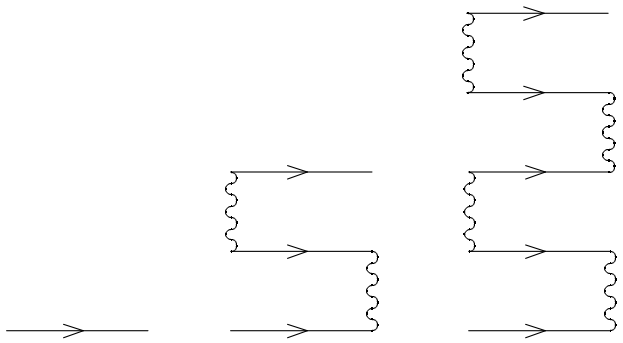

Fig. 2. A. Sherman and M.Schreiber, One-loop approximation ...

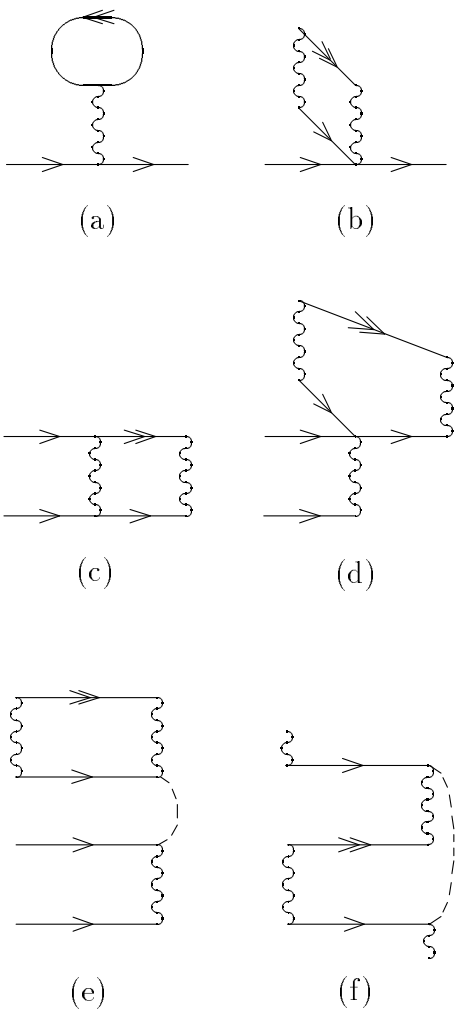

Fig. 3. A. Sherman and M.Schreiber, One-loop approximation ...

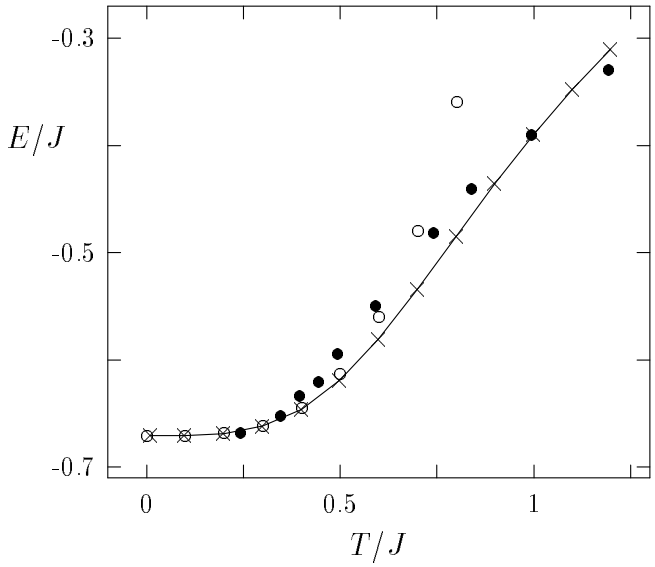

Fig. 4. A. Sherman and M.Schreiber, One-loop approximation ...

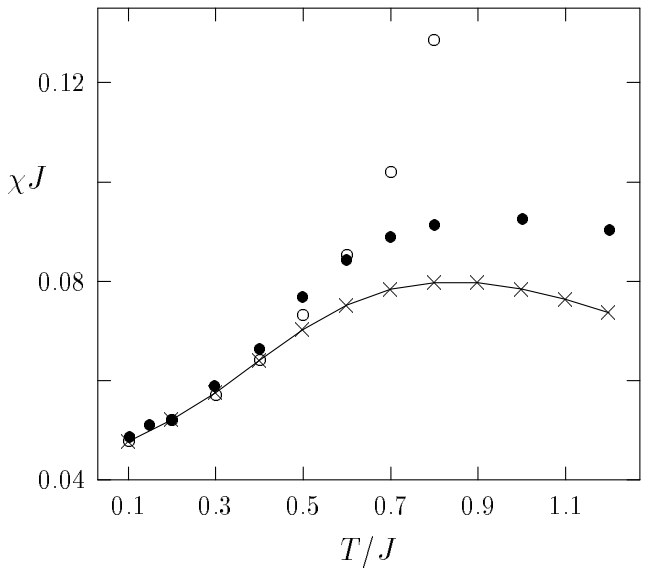

Fig. 5. A. Sherman and M.Schreiber, One-loop approximation ...

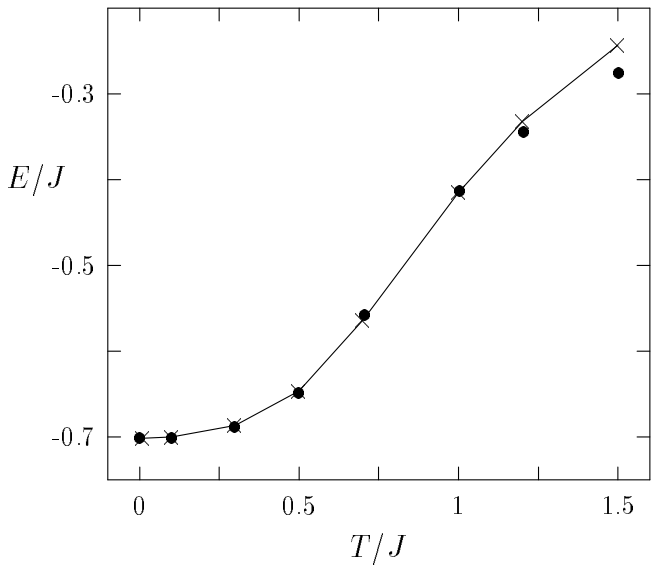

Fig. 6. A. Sherman and M.Schreiber, One-loop approximation ...